Systematic Proteome and Lysine Succinylome Analysis Reveals Enhanced Cell Migration by Hyposuccinylation in Esophageal Squamous Cell Carcinoma

Authors

Zhenchang Guo, Feng Pan, Liu Peng, Shanshan Tian, Jiwei Jiao, Liandi Liao, Congcong Lu, Guijin Zhai, Zhiyong Wu, Hanyang Dong, Xiue Xu, Jianyi Wu, Pu Chen, Xue Bai, Dechen Lin, Liyan Xu, Enmin Li, and Kai Zhang

Correspondence

lyxu@stu.edu.cn; nmli@stu.edu.cn; kzhang@tmu.edu.cn

In Brief

The proteome, phosphorylome, lysine acetylome, and succinylome were quantified for esophageal squamous cell carcinoma (ESCC) and matched control cells. Our results identify hyposuccinylation in cancer cells and reveal that ESCC malignant behaviors are inhibited once the level of succinylation was restored *in vitro* or *in vivo*, which is further confirmed in primary ESCC specimens. Our findings demonstrate that lysine succinylation may alter ESCC metabolism and migration, providing a new insight into the functional significance of posttranslational modification in cancer biology.

Graphical Abstract
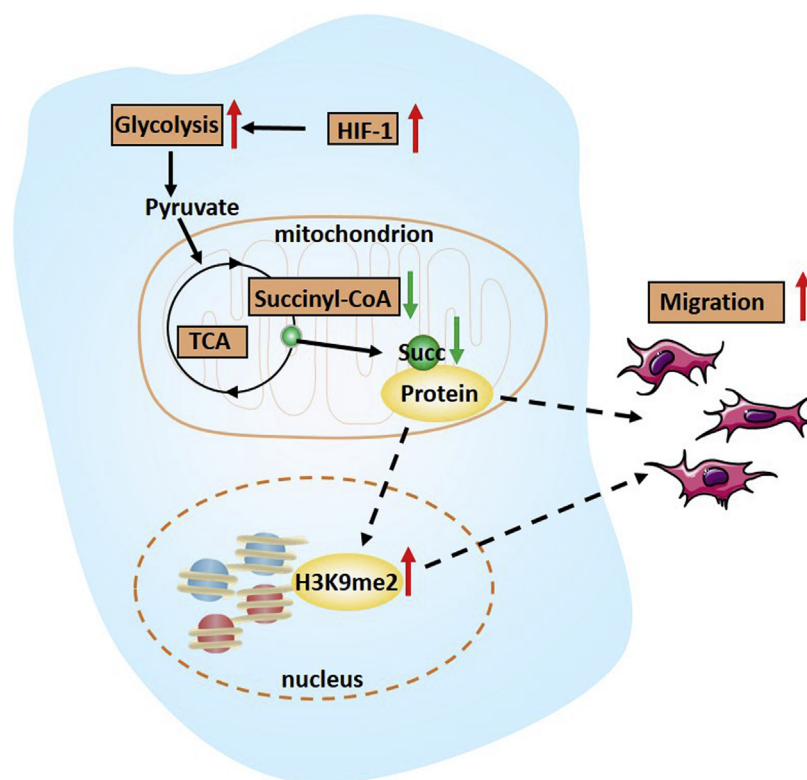
Highlights

- Quantitative proteomes, lysine acetylome, and succinylome of SHEEC and SHEE cells.

- Lysine succinylation is significantly downregulated in SHEEC cells.

- ESCC malignant behaviors are inhibited once the level of succinylation is restored.

- Hyposuccinylation is confirmed in primary ESCC specimens.

Systematic Proteome and Lysine Succinylome Analysis Reveals Enhanced Cell Migration by Hyposuccinylation in Esophageal Squamous Cell Carcinoma

Zhenchang Guo[1,2,‡], Feng Pan[2,‡], Liu Peng[2,3], Shanshan Tian[1], Jiwei Jiao[2,3], Liandi Liao[2,4], Congcong Lu[5], Guijin Zhai[1], Zhiyong Wu[6], Hanyang Dong[1], Xiue Xu[2,4], Jianyi Wu[2,3], Pu Chen[1], Xue Bai[1], Dechen Lin[7], Liyan Xu[2,3,*], Enmin Li[2,*], and Kai Zhang[1,*]

Esophageal squamous cell carcinoma (ESCC) is an aggressive malignancy with poor therapeutic outcomes. However, the alterations in proteins and posttranslational modifications (PTMs) leading to the pathogenesis of ESCC remain unclear. Here, we provide the comprehensive characterization of the proteome, phosphorylome, lysine acetylome, and succinylome for ESCC and matched control cells using quantitative proteomic approach. We identify abnormal protein and PTM pathways, including significantly downregulated lysine succinylation sites in cancer cells. Focusing on hyposuccinylation, we reveal that this altered PTM was enriched on enzymes of metabolic pathways inextricably linked with cancer metabolism. Importantly, ESCC malignant behaviors such as cell migration are inhibited once the level of succinylation was restored *in vitro* or *in vivo*. This effect was further verified by mutations to disrupt succinylation sites in candidate proteins. Meanwhile, we found that succinylation has a negative regulatory effect on histone methylation to promote cancer migration. Finally, hyposuccinylation is confirmed in primary ESCC specimens. Our findings together demonstrate that lysine succinylation may alter ESCC metabolism and migration, providing new insights into the functional significance of PTM in cancer biology.

Esophageal cancer, approximately 70% of which occurs in China, is one of the main leading causes of cancer death (1). As the major subtype of this cancer (over 90%), esophageal squamous cell carcinoma (ESCC) is highly aggressive with a 5-year survival rate of only 10% (2). Unfortunately, such low outcome has only been slightly improved over the last decades. Recent large-scale genome profiling has identified a number of driver mutations and key pathways associated with ESCC (3, 4). However, these genome characterizations have not improved clinical management of ESCC patients, and no effective targeted therapy has been established (5). Discovery of pathological alterations in proteins and posttranslational modifications (PTMs) may help advance drug development as after all, the vast majority of current drug targets are proteins.

Lysine residue is subjected to a variety of PTMs such as methylation and acetylation. Accumulated evidence suggests that modified lysine PTMs can alter protein functions (6, 7). Thus dysregulation of lysine PTMs plays important roles in cancer (8). For example, histone lysine methylation has been associated with the progression of ESCC (9). Systematic and comprehensive insights into the abnormal lysine PTMs are thus needed to advance significantly our understanding of tumorigenesis.

Recent advances in mass spectrometry (MS) technology have expanded the scope, robustness, and reliability of proteomics quantification (10). Comprehensive proteomic analyses are now capable of identifying thousands of proteins and PTMs (11), and thus substantially contribute toward the understanding of complex tumorigenic pathways on protein and PTM levels (12).

Here, we carried out a quantitative analysis of the proteome, phosphorylome, lysine acetylome, and lysine succinylome for

immortalized but nonmalignant human esophageal epithelial cell line SHEE and its malignantly transformed counterpart SHEEC. In addition to the identification of abnormal protein pathways, we noted significant downregulation of lysine succinylation in ESCC cells relative to nonmalignant control. Bioinformatic analysis further demonstrated that aberrant decrease of succinylation was enriched in key metabolic pathways, particularly in the metabolic enzymes of TCA cycle. The measurement of the donor and regulated enzymes suggests that hyposuccinylation may attribute to the decrease of succinyl-CoA, leading to the abnormal metabolism in ESCC. Further functional assays through either chemical or genetic approaches provided strong evidence that hyposuccinylation regulated the migratory ability of ESCC cells both *in vitro* and *in vivo*. Finally, we found that the degree of lysine succunylation was higher in adjacent nonmalignant esophagus epithelium than cancer tissues. Together, this work characterizes protein hyposuccinylation as a crucial PTM regulating both metabolism and migration of ESCC cells.

EXPERIMENTAL PROCEDURES
Cell Culture, Protein Extraction and Digestion

SHEEC and SHEE cell lines were grown in DMEM/F12 1:1 medium (Gibco). KYSE150 and KYSE510 cell lines were in RPMI1640 medium (Hyclone), supplemented with 10% FBS (Gibco), 2 mM L-glutamine, 15 mM HEPES, and 1% penicillin/streptomycin. For stable isotope labeling with amino acids in cell culture (SILAC) labeling, cells were cultured in DMEM/F12 1:1 medium (Thermo) containing either L-lysine (light label) or l-lysine-13C6 (heavy label). All cells were cultured at 37 °C in a humidified incubator at 5% CO2.

Cells were first lysed with cell lysis buffer (1% NP-40, 0.1% SDS, 50 mM Tris-HCl, 5 mM dithiothreitol, 2 mM EDTA, 3 μM TSA, 50 mM nicotinamide, pH 8.0, 1% cocktail III) at 4 °C for 1 h, and then the supernatants were collected after centrifuge at 12,000*g* for 3 min. After concentration was measured using BCA PROTEIN ASSAY KIT (Thermo Scientific, 23250), labeled proteins were mixed at 1:1 for SILAC experiments, and the crude proteins were precipitated by adding trifluoroacetic acid (TFA) with 25% final concentration (v/v). After washing twice with –20 °C acetone, the proteins pellets were dissolved in 100 mM NH4HCO3 (pH 8.0) for digestion. Protein solution was subjected to tryptic digestion at 37 °C for 16 h. Dithiothreitol was added to final concentration 5 mM followed by incubation at 56 °C for 30 min. Iodoacetamide was added to alkylate proteins with final concentration 15 mM followed by incubation at room temperature in dark for 30 min. The alkylation reaction was quenched by 30 mM of cysteine (final concentration) at room temperature for another 30 min. Trypsin was then added again with a ratio of trypsin to protein at 1:100 (w/w) for digestion at 37 °C for 4 h to complete the digestion.

Fraction of Peptides by HPLC and Enrichment of Modified Peptides

Digested protein samples were loaded onto reversed-phase C18 Sep-Pak columns (Waters), pre-equilibrated with 5 ml acetonitrile and 2 × 5 ml 0.1% TFA. Peptides were washed with 0.1% TFA and H2O, eluted with 50% acetonitrile (ACN). The sample was then fractionated into fractions by high pH reverse-phase HPLC using Agilent 300

Extend C18 column (5 μm particles, 4.6 mm ID, 250 mm length). Briefly, peptides were first separated with a gradient of 2%–60% acetonitrile in 10 mM ammonium bicarbonate pH 10 over 80 min into 80 fractions, Then, the peptides were combined into seven fractions and dried by vacuum centrifuging.

To enrich lysine succinylation and lysine acetylation peptides, tryptic peptides dissolved in NETN buffer (100 mM NaCl, 1 mM EDTA, 50 mM Tris-HCl, 0.5% NP-40, pH 8.0) were incubated with prewashed antibody beads (PTM Biolab) at 4 °C overnight with gentle shaking. The beads were washed four times with NETN buffer and twice with ddH2O. The bound peptides were eluted from the beads with 0.1% TFA. The eluted fractions were combined and vacuum-dried. The resulting peptides were cleaned with C18 ZipTips (Millipore) according to the manufacturer's instructions, followed by LC-MS/MS analysis.

For phosphorylated peptides enrichment, we followed the previous report (13), and both TiO2 and IMAC materials were used. Briefly, peptides were dissolved in 80% acetonitrile (ACN) and 6% TFA and incubated with TiO2 or IMAC beads (1:5 peptides to bead ratio) for 20 min. The beads were washed with 80% ACN and 0.1% TFA, and phosphopeptide elution was carried out under basic pH using ammonia.

LC-MS/MS Analysis

Peptides were dissolved in 0.1% FA, directly loaded onto a reversed-phase precolumn (Acclaim PepMap 100, Thermo Scientific). Peptide separation was performed using a reversed-phase analytical column (Acclaim PepMap RSLC, Thermo Scientific). The gradient was comprised of an increase from 6% to 23% solvent B (0.1% FA in 98% ACN) for 24 min, 23% to 35% for 8 min, and climbing to 80% in 4 min, then holding at 80% for the last 4 min, all at a constant flow rate of 280 nl/min on an EASY-nLC 1000 UPLC system, the resulting peptides were subjected to NSI source followed by tandem mass spectrometry (MS/MS) in Q Exactive Orbitrap mass spectrometer (Thermo Fisher Scientific) coupled online to the UPLC. Intact peptides were detected in the Orbitrap at a resolution of 70,000. Peptides were selected for MS/MS using NCE setting as 30; ion fragments were detected in the Orbitrap at a resolution of 17,500. A data-dependent procedure that alternated between one MS scan followed by 20 MS/MS scans was applied for the top 20 precursor ions above a threshold ion count of 1.5E4 in the MS survey scan with 30.0 s dynamic exclusion. For MS scans, the m/z scan range was 350 to 1800.

Database Search

For the quantitation of proteome, succinylome, acetylome, and phosphorylome, we used SILAC strategy. The resulting MS/MS data was processed using MaxQuant (v.1.5.5.1). Tandem mass spectra were searched against Uniprot human (20,205 entries, download at 2017.06.17) database concatenated with reverse decoy database. Trypsin/P was specified as cleavage enzyme allowing up to two missing cleavages. Mass error was set to 10 ppm for precursor ions and 0.02 Da for fragment ions. Carbamidomethylation on cysteine was specified as fixed modification and oxidation on Met, acetylation on protein N-terminal were specified as variable modifications, Phosphorylation on serine, threonine, and tyrosine and succinylation or acetylation on lysine were set as variable modifications respectively. False discovery rate (FDR) thresholds for protein, peptide, and modification site were specified at 1%. Minimum peptide length was set at 7 and "match between runs" was enabled. All the other parameters in MaxQuant were set to default values.

MaxQuant search results from different jobs were exported and combined; modified peptides with score less than 60 and localization probability score less than 0.75 were removed (14). And the threshold

of the up- or downregulated proteins or PTM sites level was set as twofold change.

Bioinformatic Analysis

The majority of the bioinformatics was accomplished by using Perseus and Microsoft Excel. Gene Ontology (GO) enrichment analysis and pathway enrichment analysis were carried out by using DAVID and WebGestalt (15). The String database version 10 was read into Cytoscape for visualization of GO items and protein–protein interactions. Statistical analyses were performed using SPSS 19.0 software (SPSS). Survival was estimated by Kaplan–Meier survival analyses with the log-rank test. Associations of Ksucc and clinicopathological characteristics were assessed with Fisher exact test. For the above comparisons, a two-tailed p value less than 0.05 was considered statistically significant.

Extraction of Metabolites from SHEEC and SHEE Cell Lines

For metabolites from the TCA and glycolysis pathways extraction, we used 80% methanol to extract. In brief, cells were washed by using ice-cold PBS buffer three times gently and 2 ml 80% (vol/vol) methanol (prechilled to −80 °C) was added to the plates, and the plates were incubated at −80 °C for 1 h. Then the plates were scraped on dry ice with cell scraper. The tube was centrifuged at 14,000g for 20 min at 4 °C, and the metabolite-containing supernatant was transferred to a new tube on dry ice. SpeedVac was applied to pellet using no heat, and the dried samples were stored in −80 °C freezer for MS analysis.

For the succinyl-CoA and acetyl-CoA extraction, we followed the previous reports (16). Cells were washed by using ice-cold PBS buffer three times gently and briefly spun down at 1000g. Then cells were resuspended in 1 ml of ice-cold extraction solution (10% [wt/vol] TCA), and cells were sonicated for 30 s on ice at a rate of 1 pulse per second. The sonicated cell lysate was spun at 15,000g for 5 min at 4 °C to precipitate the protein pellet. And then the Oasis HLB SPE columns (Waters, cat. no. WAT094225) were conditioned with 1 ml of methanol, after that columns were equilibrated with 1 ml of water. Acid-extracted lysate (supernatant) was loaded onto the columns and washed with 1 ml of water. CoA compounds were eluted into fresh tubes by three subsequent applications of 0.5 ml of 25 mM ammonium acetate in methanol. Finally, the samples were dried with the Speedvac.

Western Blot Assay

For Western blot, cells were washed with PBS and lysed with modified RIPA. Chemical treatments of cells were carried out by supplementing the chemicals directly into culture media. Western blotting was carried out by employing standard methods. And the pan-antibody was purchased from PTM Biolabs.

Aldolase Enzymatic Assay

The enzyme activity of aldolase in whole cell was measured by an enzymatic colorimetric assay kit (sigma, MAK223) according to the manufacturer's instructions. The aldolase activity of permeabilized cells was measured as described. Briefly, cells grown in six-well plates, were washed with PBS for two times, and then incubated in 30 μg/ml digitonin/PBS for 5 min at 4 °C. After incubation, the supernatant was collected and cells were lysed in 200 μl RIPA buffer. The supernatant was centrifuged at 2000 rpm to remove cellular components. The cell supernatant was mixed with 200 μl hydrazine (0.0035 M), 6 μl iodoacetate (0.01 M), 3 L EDTA (0.01 M), and to make a final volume of 300 μl with lysis buffer. A blank read was taken at 240 nm, then 10 μl of 0.12 M FBP was added, and absorption was detected at 240 nm in 5 min intervals for three readings. Mean

enzymatic activity was determined according to the methods provided in the reference (17).

Plasmids and Transfection

The plasmids pCMV3-PCK2-Flag, pCMV2-ACO2-Flag, and pCMV3-FH-Flag were purchased from Sino Biological Inc. A Fast Mutagenesis System Kit (TransGen Biotech) was used to generate site-specific mutations, at PCK2 lysine 108, ACO2 lysine 739, and FH lysine 115, according to the manufacturer's instructions. Detailed information about primers used for mutagenesis is listed supplemental Table S1. K-to-R mutants were mimicking the desuccinylated state or K-to-E mutants mimicking the negatively charged succinyllysine modification. KYSE150 and KYSE510 cells were transfected, using Lipofectamine 3000 (Invitrogen) according to the manufacturer's instructions.

Wound Healing Assays

Wound healing assays were performed as described previously (18). Confluent cultures in a six-well plate were incubated in serum-free medium for 12 h to achieve quiescence. Circles 3 mm in diameter were marked on the bottom of each dish to identify the areas for image capture and ensure that measurements were taken at the same locations. A wound was made by scratching the monolayer, with a sterile pipette tip through the circled areas, then cells were rinsed twice with phosphate-buffered saline and referred with the medium supplemented with 2% FBS. Phase-contrast micrographs of the circled areas were taken immediately after refeeding and after 24 h and 36 h incubations at 37 ℃. The distance of migration was calculated from six images, using ImageJ analysis. Cell velocity was calculated by taking five random, evenly spaced measurements along each wound length and averaged to determine wound width.

Migration Assay

Migration assays were performed as described previously (19). Briefly, cells (5 × 104) were plated in medium without serum in the upper well of a transwell chamber of a 24-well transwell with 8-μm pores (BD Biosciences), placed in a bottom chamber containing medium supplemented with 10% fetal bovine serum. After 48 h, the membranes were fixed and stained with haematoxylin solution, and migration was quantified by counting ten random fields under a light microscope (400×). The mean value was calculated from data obtained from three separate chambers.

Quantification of Histone PTMs

Histone extraction and quantitation analysis was performed as previously described (20). Briefly, histones were acid-extracted from nuclei with 0.2 mM H_2SO_4 for 8 h and precipitated with 25% trichloroacetic acid for 0.5 h. Purified histones were then derivatized with propionic anhydride twice as previously reported (20). Briefly, we added 10 μl fresh propionylation reagent (by mixing propionic anhydride with acetonitrile in the ratio 1:3 [v/v]) into 40 μl histone samples. And then NH_4OH was quickly added to re-establish pH 8.0 to the solution. The pH will be checked after mixing the solution by vortex. Then, samples were incubated at room temperature for 15 min. Finally, samples were dried out completely, and the steps were repeated again. After these steps, histones were then digested with trypsin (enzyme: sample ratio 1:20, 37 °C, 16 h) in 50 mM NH_4HCO_3. After digestion, we resuspended samples in 40 μl of 100 mM NH_4HCO_3, the derivatization reaction was then performed again twice as described before in order to derivatize peptide N-termini. Samples were then desalted with using C18 Stage-tips for LC-MS analysis. The HPLC gradient was as follows: 6%–45% solvent B (A = 0.1% FA; B =80% ACN, 0.1% FA) over 55 min, from 45% to 100% solvent B in 5 min,

100% B for 10 min at a flow rate of 300 nl/min. The nanoLC was coupled to a Q Exactive Plus (Thermo Fisher Scientific). A full-scan MS spectrum (m/z 300–1100) was acquired and the entire mass range was fragmented at every cycle using windows of 50 m/z. For histone PTMs, we used data-independent acquisition (DIA) mode to acquire the raw data and LFQ methods for quantitation. EpiProfile 2.0 was used to calculate the relative abundance of each peptide as compared with the total respective histone, referred to the previous report (21).

Patients and Specimens

For the retrospective study, 106 cases of formalin-fixed, paraffin-embedded ESCC tissue specimens and 97 cases of adjacent normal esophageal tissues were collected between January and December, 2011, at the Shantou Central Hospital. All tumors were confirmed as ESCC by pathologists in the Clinical Pathology Department of the Hospital, and the cases were classified according to the eighth edition of the tumor-node metastasis (TNM) classification system of the International Union against Cancer. Evaluation of tumor differentiation was based on histological criteria of the guidelines of the WHO Pathological Classification of Tumors. Information on age, sex, and histopathologic factors was obtained from the medical records.The follow-up for patients after esophageal resection was continued until their deaths, and only patients died from ESCC were included in the tumor-related deaths. Follow-up extended to January, 2017. The study was approved by the Ethics committee of the Center Hospital of Shantou City, the local ethics committee, and only patients with written informed consent were included.

Tissue Microarray Construction and Immunohistochemical Analysis

Tissue microarray (TMA) construction of esophageal carcinoma tissue has been described earlier (22). TMA sections were sectioned (4 µm) and incubated with rabbit-derived pan lysine succinylated antibody (1:2000; PTM-401, PTM BioLab). Immunohistochemistry (IHC) was performed using a two-step protocol (PV-9000 Polymer Detection System; ZSGB-BIO) according to the manufacturer's instructions and has been described in our previous studies (23). Slides were scanned using the PerkinElmer Vectra and images were analyzed using the inForm software (PerkinElmer, Hopkinton, MA) (24, 25). For statistical analysis, the protein expression score was divided into two subgroups, high-expression and low-expression, on the basis of X-tile software analysis.

Tumor Xenograft Model

All animal studies were conducted in accordance with protocols approved by the Animal Research Committee of the Shantou Administration Center. Five-week-old male Nude/Nude mice were purchased from Vital River Laboratories and given water and food ad libitum. Suspensions of 1×10^6 SHEEC/Control or SHEEC/DMS cells (Treatment of cells with 10 mM DMS for 48 h before inoculation) in 100 µl of culture medium (DMEM or DMEM with 10 mM DMS) were injected into the right footpad (n = 5 mice each group). Tumor growth was monitored and tumor size was measured every three 3 days following the appearance of tumors at about 14 days after injection. At 30 days after injection, mice were sacrificed, and tumors were excised and weighed, then preserved in formalin for histological analysis (26).

Experimental Design and Statistical Rationale

In this study, we performed quantitative proteomics based on SILAC methods to test the difference between SHEEC and SHEE cells. For protein quantitation, three biological replicate experiments were performed, and each experiment was separated ten fractions by HPLC. For acetylome and succinylome enrichment, we performed two biological replicate experiments, and each experiment was separated seven fractions by HPLC. For phosphorylome quantitation, we used both IMAC and TiO_2 materials to enrich, and each experiment was performed two biological replicates, also each experiment was separated ten fractions by HPLC. For histone PTMs quantitation, we performed two biological replicate experiments, and five technical replicates were performed in each experiment. T-test and F-test were used in the study of histone PTMs, and p-value smaller than 0.05 was considered as significantly regulated.

RESULTS

Quantitative Proteomic Analysis of SHEEC and SHEE Cell Lines

Our previous studies have established the paired SHEE (nonmalignant) and SHEEC (malignant) lines as cell models for investigation of ESCC biology (3). SHEE is similar to a primary cell line and retains its proliferation ability and differentiation potential. SHEEC was established through induction of the SHEE cell line using 12-otetradeanoy-lphorbol-13-acetate (TPA). These twocell lines are the most appropriate models for ESCC tumorigenesis (27, 28). In the present study, we first verified their phenotypical features through a series of *in vitro* and *in vivo* assays (See Experimental Procedures). As shown in supplemental Figure S1, *A–C*, SHEE retains the phenotype of primary epithelial cells, such as growth in a monolayer and anchorage-dependent cell aggregation without colony formation in soft agar or tumor formation after transplantation, while SHEEC exhibits strong tumorigenicity. The two cell lines were used to investigate both the proteome and PTMs.

We applied quantitative proteomics techniques based on SILAC approach to profile the proteome in both cell lines (supplemental Fig. S2A and supplemental Table S2), and we were able to quantify a total of 3814 proteins. Excellent correlations among three replicates (average Spearman rank correlation coefficient was 0.92, supplemental Fig. S2B) highlighted the robustness and reliability of these results. Among these 3814 proteins, 297 were upregulated (fold change >2 increase) and 152 downregulated (fold change >2 decrease) (Fig. 1A and supplemental Table S2). We next compared the proteome and matched mRNA quantification in these two cell lines (supplemental Fig. S3A and supplemental Table S3). In agreement with previous findings (12, 29), the alterations at the protein level were not completely concordant with that of mRNA, indicating that extensive post-transcriptional and posttranslational processes both can only be captured by proteomic approaches. A number of known functional factors associated with ESCC were readily observed in the list of differentially expressed proteins, such as Ezrin, GRB2, and RB1 (3, 30). We next systematically interrogated these differentially expressed proteins for their functional classification, protein–protein interaction networks as well as pathway enrichment using GO classification and the KEGG pathway analysis (supplemental Fig. S3B and supplemental Table S4). Notably, a number of known
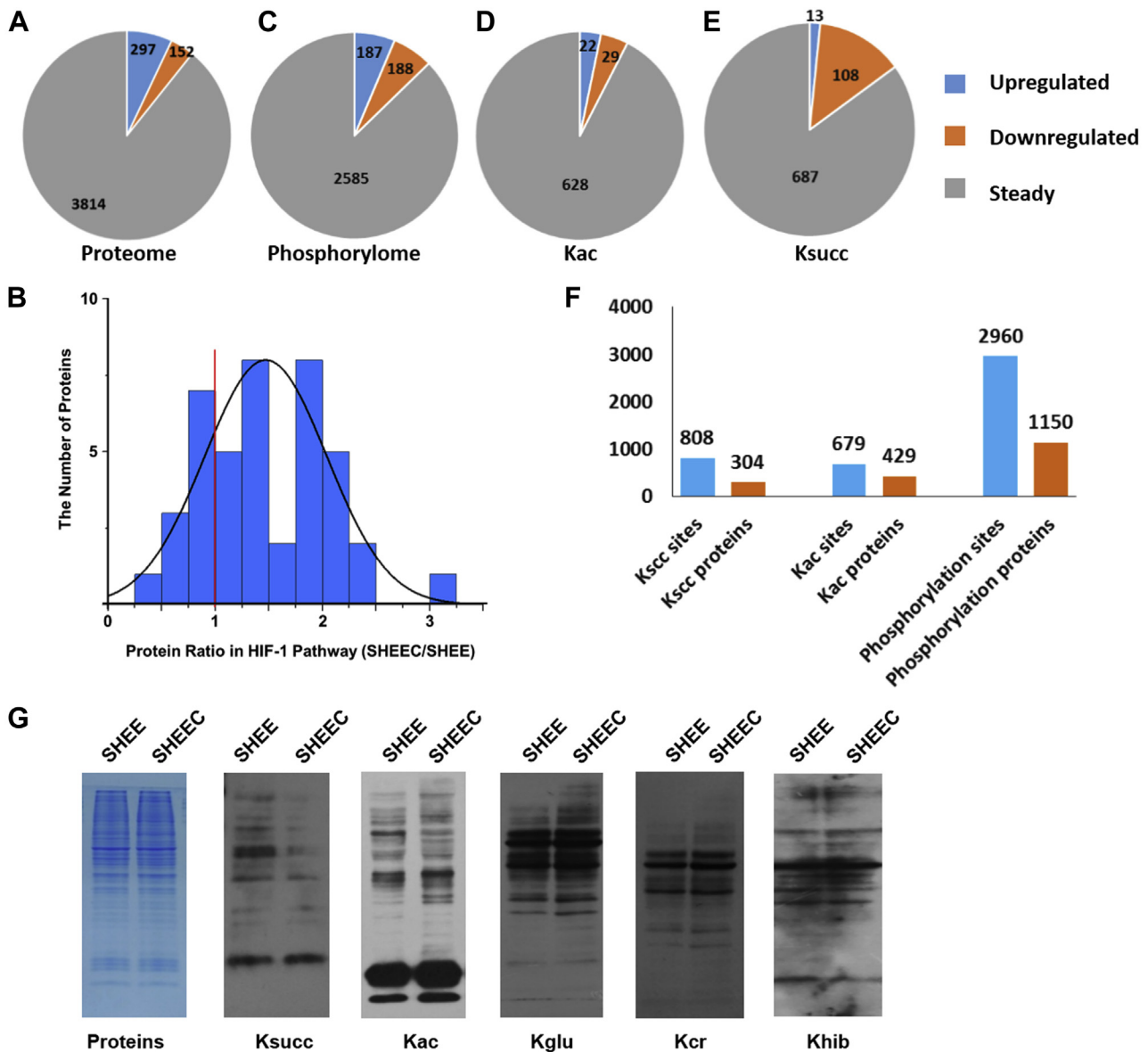
FIG. 1. **Quantitation and verification of proteomics and PTMs.** *A, C, D, E*, quantifications of proteome, phosphorylome, lysine acetylome, and lysine succinylome between SHEEC and SHEE using SILAC approach, respectively. *B*, the quantitative analysis of proteins in HIF-1 between SHEEC and SHEE. *F*, the amounts of modified proteins and sites identified in SHEEC and SHEE. *G*, Western blotting analysis for proteomics and short-chain lysine acylations between SHEEC and SHEE.

pathways involved in cancer biology were identified, including HIF-1 signaling, glycolysis, and oxidative phosphorylation.

Abnormal Protein Pathways in SHEEC Cells

As mentioned above, pathway analysis of differentially expressed proteins showed that the HIF-1 signaling was strongly enriched. Meanwhile, GO analysis demonstrated that the expression of metabolic enzymes was highly dysregulated. HIF-1 signaling is known to stimulate glycolysis and repress mitochondrial functions (31), contributing to cancer initiation and development. The majority of proteins in these pathways were increased in SHEEC cells (Fig. 1*B* and supplemental

Fig. S3*C* and supplemental Table S5), suggesting that HIF-1 signaling and glycolysis pathways were activated in ESCC, in agreement with previous reports (31–33).

Recent studies showed that the activity of HIF-1 signaling was regulated by protein phosphorylation (33), lysine acetylation (34), and lysine succinylation (32). Moreover, these PTM processes are dependent on the molecule donors from metabolic pathways. For example, most of donors of lysine acetylation and lysine succinylation (acetyl-CoA and succinyl-CoA) are derived from products in TCA cycle. These findings together prompted us to investigate these three forms of PTMs in our cell line model.

Quantitative Proteomics on PTMs Reveal that Lysine Succinylation Is Decreased Significantly in Cancer Cells

To determine the global level of protein phosphorylation, lysine acetylation, and lysine succinylation in SHEE and SHEEC cells, we performed quantitative proteomics screening of phosphorylated-, acetylated-, and succinylated-peptides using SILAC labeling, protein fractionation, affinity enrichment, and HPLC-MS/MS analysis (supplemental Figs. S2A and S4A and supplemental Tables S6–S8). As a result, we identified a total of 7588 sites with phosphorylation (in 2708 proteins), 755 with acetylation (in 489 proteins) as well as 879 with succinylation (in 358 proteins). After applying stringent cutoff criteria and removing those peptides with overlapping amino acids, and normalized by corresponding protein ratios, we quantified 2960 sites with phosphorylation (187 upregulated and 188 downregulated), 679 with acetylation (22 upregulated and 29 downregulated), as well as 808 with succinylation (13 upregulated and 108 downregulated) (Fig. 1, C–F). The quantitative analysis of the three PTMs showed an obvious trend. While the numbers of upregulated phosphorylation and lysine acetylation sites were comparable with those of downregulated ones (Fig. 1, C and D and supplemental Fig. S4B), it was interesting to note that decreased succinylation accounted for the vast majority of all alterations in lysine succinylation in SHEEC cell line (Fig. 1E).

To confirm the above results, we used label-free quantitative proteomics approach to quantify the succinylated peptides from the two cell lines (supplemental Fig. S4C and supplemental Table S9), and similar results were obtained. Next to test if the decrease of lysine succinylation was a distinctive feature of PTM in ESCC, we performed western blot assay to measure lysine succinylation and other short-chain lysine modification, such as acetylation, crotonylation, 2-hydroxyisobutyrylation, as well as glutarylation. As shown in Figure 1G, only lysine succinylation in SHEEC was significantly lower than that in SHEE, suggesting that decrease of lysine succinylation is a unique and specific form of PTM alteration in ESCC cells.

We next analyzed the proteins displaying downregulated succinylation using GO classification, KEGG pathway as well as the STRING database. Notably, the majority of hyposuccinylated proteins were involved in the TCA cycle (Fig. 2 and supplemental Table S10).

Comprehensive Analysis of Proteome and PTMs in Metabolic Pathways

We next focused on energy metabolism pathways and compared the relative abundance of lysine succinylation, acetylation, phosphorylation, and protein expressions as well as metabolic products between SHEE and SHEEC cell lines in TCA cycle, pyruvate metabolism, and glycolysis, through targeted metabolomics method (supplemental Tables S11–S13).

As shown in Figure 2 and supplemental Figure S4D, the expression of metabolic enzymes and metabolic products in glycolysis, pyruvate metabolism, and fatty acid synthesis were markedly upregulated in SHEEC, while those in TCA were not significantly changed, except for SDHA and SUCLA2 as well as metabolic products succinyl-CoA. To examine the effects of these abnormally expressed proteins on metabolism, we analyzed the enzymatic activation of fructose-bisphosphate aldolase A (ALDOA) that was markedly upregulated in SHEEC. Consistently, the ALDOA activity in whole cell lysate was increased in SHEEC (Fig. 3B), which was contributed by ALDOA in cytoplast. In addition, both the activity and expression of ALDOA were increased under serum starved condition (Fig. 3A). These results confirmed that anaerobic respiration was enhanced in SHEEC, consistent with the Warburg effect in cancer cells (35).

Low-level of Succinyl-CoA Resulted in Hyposuccinylation in ESCC Cells

At the level of PTMs, lysine succinylation was significantly decreased in proteins engaged in TCA cycle in ESCC cells (Fig. 2 and supplemental Table S10). Several factors have been suggested to contribute to the decrease of lysine succinylation, including the "eraser" SIRT5, which is the only reported desuccinylase in cytoplasm (36, 37). However, the expression of SIRT5 in SHEEC was similar to that of SHEE (fold changes of protein and mRNA were 1.16 and 0.88, respectively). A previous study also showed that lysine succinylation was regulated by succinyl-CoA concentration (38). In our metabolic analysis, the relative abundance of succinyl-CoA decreased potently (ratio SHEEC/SHEE = 0.55, supplemental Fig. S5B). These data suggest that the decrease of lysine succinylation may be caused by the reduction of succinyl-CoA level in SHEEC cells.

Increased Lysine Succinylation Inhibits the Migration of SHEEC Cells

Besides the TCA cycle, downregulated succinylation also was enriched in other pathways involved in tumor biology, including oxidative phosphorylation, propanoate, and fatty acid metabolism. These metabolism pathways are believed to associate with the regulation of tumor behavior such as migration (supplemental Fig. S5A and supplemental Table S10) (39). Thus we next performed cellular phenotypical assays to investigate the functional relevance of lysine succinylation in ESCC. We first increased the global level of lysine succinylation by addition of dimethyl-succinate (DMS) in SHEEC cells (40) (Fig. 3C and supplemental Fig. S6). Importantly, migration ability of SHEEC cells was inhibited potently with the increase of lysine succinylation as measured by both wound healing and trans-well assays (Fig. 3, D and E). Similar results were obtained from another ESCC cell line, KYSE150. This data indicates that hyposuccinylation may promote the capability of migration in ESCC cells.
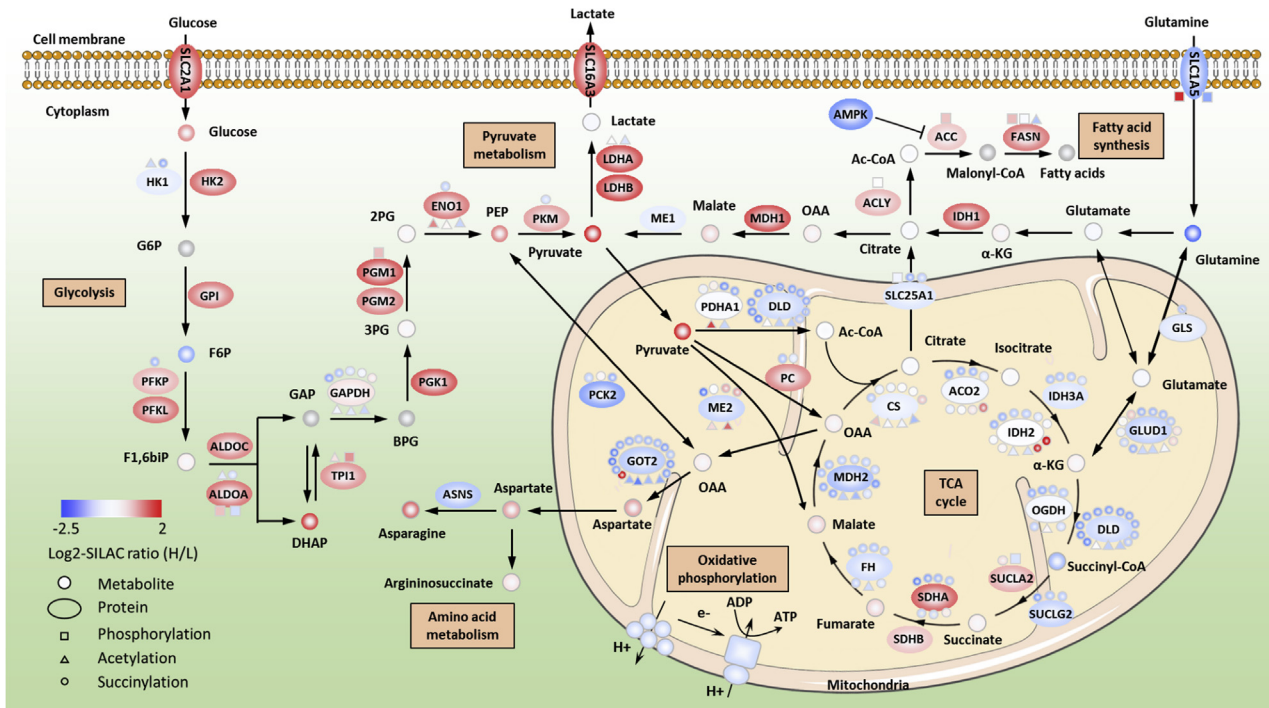
FIG. 2. **Abnormal metabolic pathways.** Proteins, PTMs, and metabolites were described with different shapes. The *red color* represents upregulated while the green representative downregulated. A majority of the proteins in glycolysis pathway were upregulated, and most of the lysine succinylation were downregulated in TCA pathway.

Mutations on Lysine Succinylation Sites Affect the Migration of SHEEC

To further explore the mechanisms of lysine succinylation in cancer cell biology, we investigated the functions of specific succinylated sites. Based on the proteomic analysis, we chose three hypo-succinylated proteins in SHEEC including phosphoenol pyruvatecarboxykinase 2 (PCK2), aconitate hydratasemitochondrial (ACO2), and fumarate hydratase (FH), which have been reported to regulate tumor phenotypes (41–43). We performed site-specific mutagenesis to generate either K-to-R mutants (mimicking the desuccinylated state) or K-to-E mutants (mimicking the succinylated state). Importantly, the migration ability of both KYSE150 and KYSE510 cell lines was inhibited when either of the three desuccinylated mutants was introduced (Fig. 4, *A* and *B*). These results were consistent with our earlier findings obtained through DMA treatment and further suggest that lysine succinylation may regulate the function of protein substrates, thereby altering the cell migration of ESCC cells.

Hyposuccinylation Regulates Histones PTMs

Histone PTMs often played important role in the development of cancer (41). As the hypersuccinylation regulates the histone methylation (37), here we wonder if hyposuccinylation is also responsible for histone methylation, and any other histone PTM has a significant change in SHEEC cell lines. As the DMS increased the level of lysine succinylation, we carried out to stimulate SHEEC cells with various concentrations of DMS buffers. Considering the unique properties of histone proteins such as the highly intensity of lysine and arginine and combinatory PTMs, which results in that the tryptic peptides of histone were difficult in quantitation, we used a DIA mass spectrometry method for histone PTMs analysis (44). We quantified more than 230 different histone peptides including lysine methylation, acetylation, and phosphorylation (supplemental Table S14) from two individual biological replicates, and we obtained a high degree of correlation between the replicates (supplemental Fig. S8A). Notably, we found that the changes of histone PTMs in H3 and H4 are more regular (supplemental Fig. S7B), we then calculated the abundance of single PTMs in H3 and H4 to study the change rule of them with the DMS treated. By using all peptides carrying the modification, for example, to estimate globally the relative abundance of H3K9me2, we summed the relative abundances of all peptides carrying this modification (H3_9–17) (i.e., H3K9me2 + H3K9me2K14ac + H3K9me2S10ph + H3K9me2S10phK14ac), we got all the single PTMs abundance finally (Fig. 5A).

By observing the changing rules of the histone PTMs, we found that the change of some histone PTMs has certain regularity. Especially, the level of succinylation was upregulated with the increase of DMS concentration, while the H3K9me2 showed the similar downward trends (Fig. 5B). This suggests that succinylation may have a negative regulatory
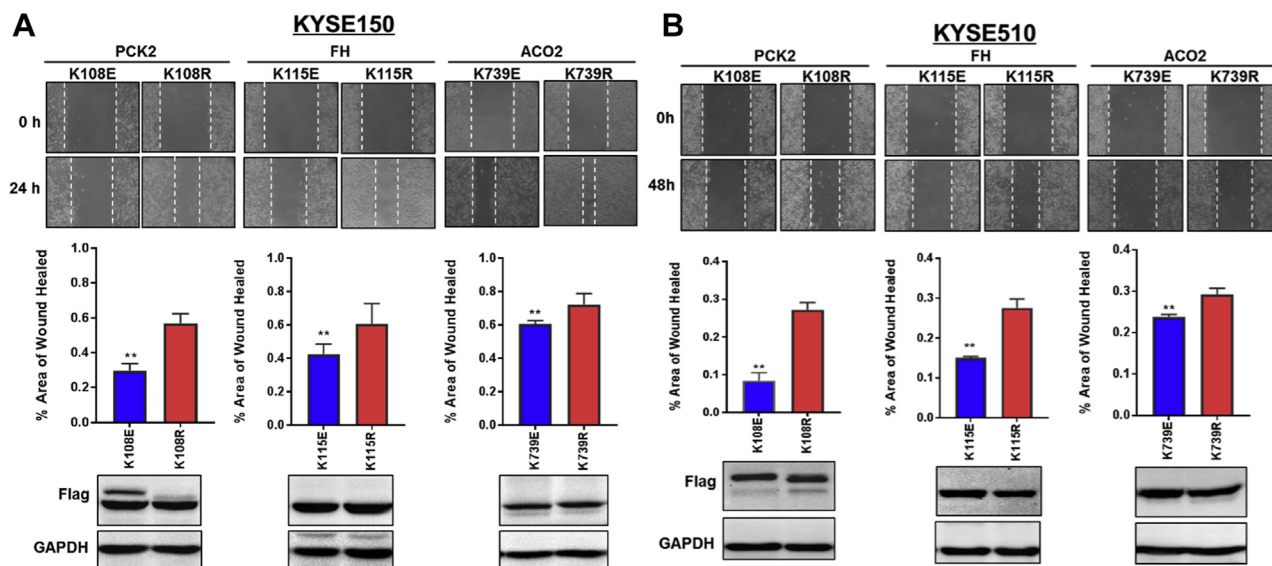
FIG. 3. **Lysine succinylation involves metabolic pathways and cell migration.** *A*, the aldolase activity of permeabilized cells in response to serum in two cells. Bar graphs represent means ± SD of three independent experiments. *B*, whole cell aldolase activity in SHEE and SHEEC cells. *C*, treatment by 10 mM dimethyl-succinate (DMS) and 100 mM glycine in SHEEC cells caused different change of the lysine succinylation level. The DMS treatment increased the level of succinylation, while the glycine reduced it. Cells were cultured in 5% FBS, and the control were mock-treated with DMSO. *D*, *E*, hypersuccinylation caused by DMS inhibited migration and. *D*, scratch experiments for the cell migration. *E*, transwell experiments for the cell migration.

effect on H3K9me2. And we then checked the expression of H3K9me2 in SHEEC and SHEE cell lines by western blot. The expression of H3K9me2 in SHEEC is higher than in SHEE cells (Fig. 5C), which is contrary to the expression of succinylation in the two cell lines. This further indicates the negative regulation of succinylation to this histone mark in SHEEC cells.

The aforementioned experiments have showed the effect of succinylation to tumor cell behaviors, thus we would like to understand what it means that this histone mark negatively regulated by succinylation. We examined the migration ability of three kinds of esophageal cancer cell lines (SHEEC, KYSE510, and KYSE150) and measured the level of H3K9me2. Just as the migration ability of the SHEEC, KYSE510, and KYSE150 cell lines is higher and higher (Fig. 5D and supplemental Fig S8B), the level of H3K9me2 also upregulates correspondingly (Fig. 5E). Collectively, these results show that hyposuccinylation changes the level of histone PTMs, which may involve the regulation of SHEEC cell migration.

DMS Inhibits ESCC Cell Growth, Migration, and Invasion in Vivo

We next explored the role of lysine succinylation in ESCC invasion *in vivo*. SHEEC cells were treated with either DMS or diluent control for 48 h before inoculation, and they were transplanted into the right footpad of nude mice. Importantly, 30 days after inoculation, the tumor sizes and weights of DMS group were significantly reduced compared with control group ($p < 0.05$) (Fig. 6, *A–E*). Moreover, in the control group, 100%

(5 of 5) of the mice exhibited local tumor invasion from footpad to ankle joint. In contrast, in the DMS group, only 40% (2 of 5) of the mice exhibited local tumor invasion (Fig. 6, *C* and *E*). Meanwhile, the succinylation level of tumor in DMS group was obviously increased compared with control group (Fig. 6B). These results strongly indicate that DMS inhibits ESCC cell growth, migration, and invasion *in vivo* through elevation of lysine succinylation.

Lysine Hyposuccinylation in Primary ESCC Specimens

Our aforementioned results promoted us to examine succinylation level in primary ESCC specimens. We collected pairs of human ESCC samples with matched adjacent nonmalignant esophagus epithelium and measured the succinylation levels in all these samples. In immunohistochemical analysis, lysine succinylation was detected mainly in the cytoplasm (Fig. 6). Importantly, the majority of nonmalignant esophagus epithelium (n = 97) exhibited intense immunostaining (Fig. 6, *F* and *G*), whereas weak staining was observed in the paired tumor tissues (n = 106) (Fig. 6, *F* and *H*). Moreover, a significant correlation was observed between low levels of succinylation level and high rate of lymph node metastasis ($p = 0.028$), supporting our earlier functional results (supplemental Fig. S5C and supplemental Table S15).

DISCUSSION

Our study comprehensively characterized ESCC-associated alterations in protein, phosphorylation, lysine acetylation, and succinylation, providing a valuable database
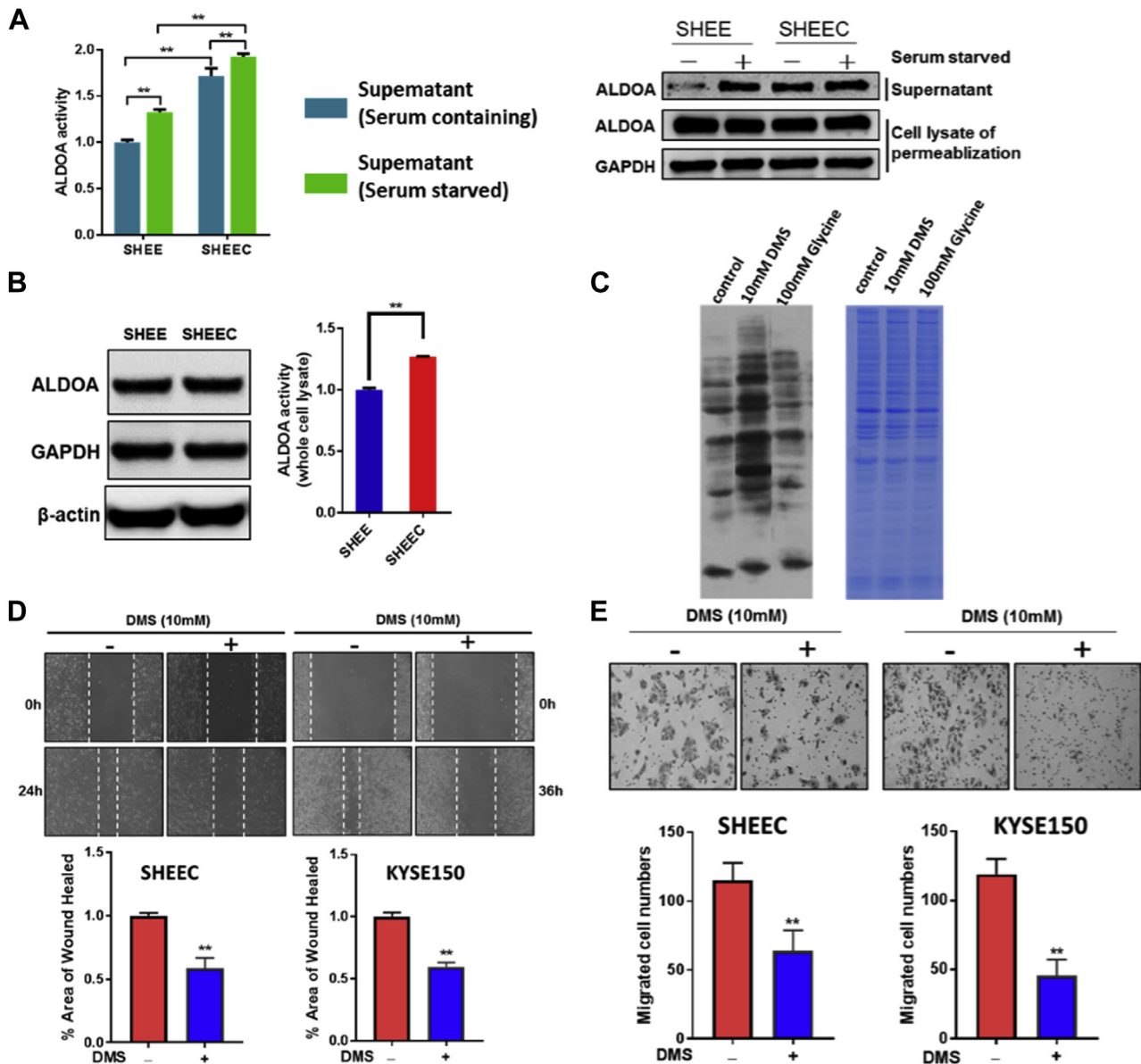
FIG. 4. **Mutations on the proteins in both ESCC cell lines KYSE150 and KYSE510.** Mutations on PCK2 (K108), ACO2 (K739), and FH (K115) inhibited cell migration obviously in two ESCC cell lines KYSE150 (*A*) and (*B*).

for further investigation of molecular mechanisms underlying ESCC tumorigenesis and progression at protein and PTM levels. Our enrichment analysis identified altered pathways and protein networks, and further investigations uncovered a functional interplay between HIF and metabolic pathways. Considering potential PTM-mediated effects on these pathways, we measured the global levels of phosphorylation, lysine acetylation, and succinylation in both SHEE and SHEEC cells, thus an interesting trend was observed. The amounts of upregulated phosphorylation and lysine acetylation sites were comparable with those of downregulated ones, while lysine succinylation was significantly downregulated in SHEEC. Further analysis confirmed the significant hyposuccinylation

on metabolic enzymes engaged in TCA in cancer cells. Recent studies have highlighted that alterations of enzyme activities affect cell metabolism and can have profound impact on cancer development (35, 45). For example, reduction of activities of FH and succinate dehydrogenase (SDH) has all been implicated as metabolic suppressor (46). Additionally, mutations in isocitrate dehydrogenase (IDH) enzymes promoted cancer aggressiveness *via* the production of oncometabolite, 2-hydroxyglutarate (d-2HG) (47). Recently, it has been recognized that lysine succinylation can alter the activities of metabolic enzymes such as IDH (48), resulting in metabolic alteration. This prompted us to ask if hyposuccinylation has functional impact on metabolic processes in ESCC cells.
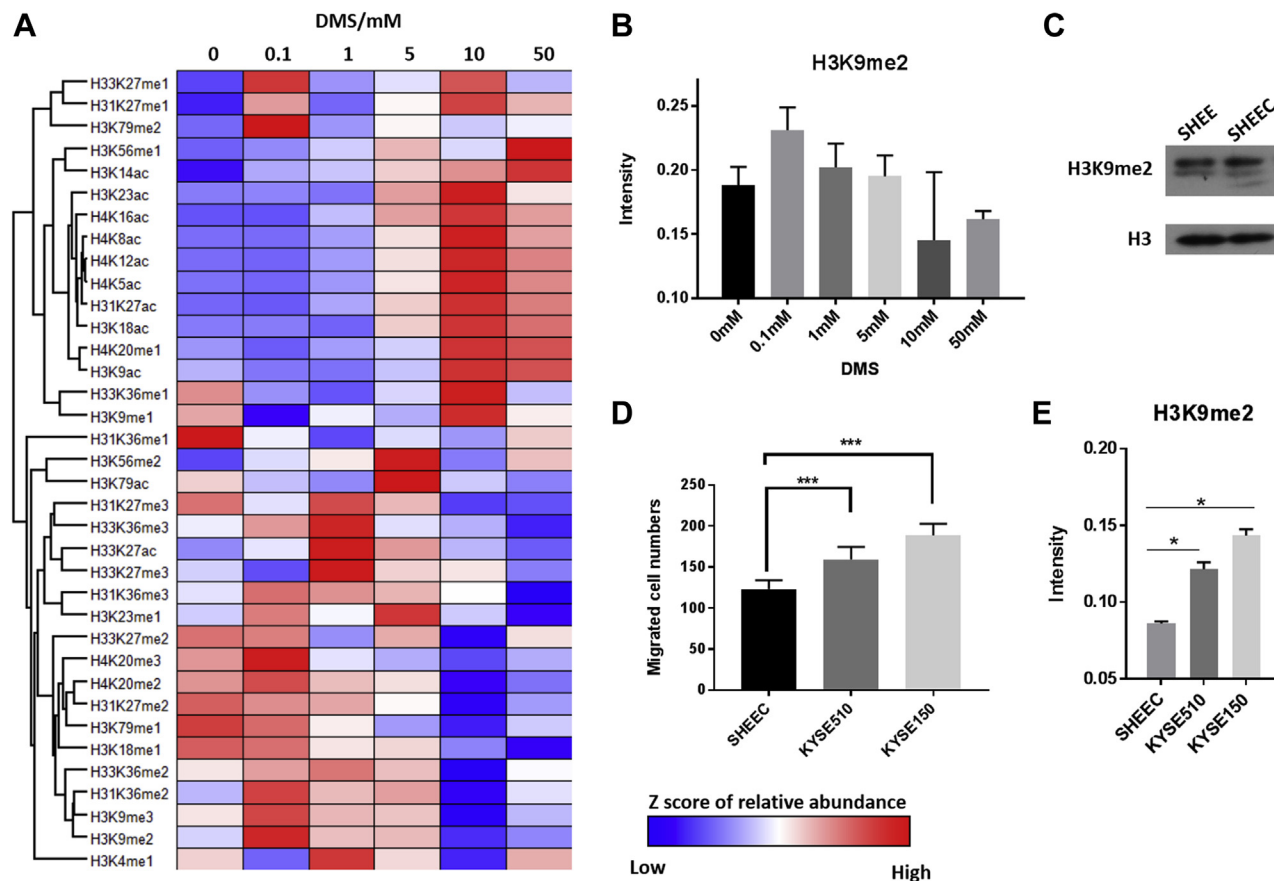
Fig. 5. Hyposuccinylation regulates histones PTMs. *A*, heatmap of the single PTMs in H3 and H4 in SHEEC cells treated with different concentrations, the data set was obtained from two bioreplicates and every bioreplicate performed three technical replicates, the FDR was set to 0.05. *B*, the variation trend of H3K9me2 with the DMS rised. *C*, validation of H3K9me2 by western blot in SHEEC and SHEE cell lines. *D*, the cell migration ability of the SHEEC, KYSE510, and KYSE150 cell lines. *E*, the variation trend of H3K9me2 in the SHEEC, KYSE510, and KYSE150 cell lines.

Further genetic perturbation (through site-specific mutagenesis of succinylation sites) and chemical approach (DMS treatment) demonstrated that the altered succinylation indeed affected the migratory ability of ESCC cells.

Warburg effect is featured by enhanced glycolysis and repressed mitochondrial functions in cancer cells (49). In keeping up with this well-known characteristic, our data showed that enzymes involved in glycolysis and their metabolic products were significantly upregulated in SHEEC cells. On the other hand, enzymes responsible for TCA cycle were slightly reduced, while their succinylation was significantly downregulated. At the level of proteins, metabolic isoenzymes showed significant and tumor-specific expression changes (50). At the level of PTMs, our work indicates that hyposuccinylation of enzymes may be a key mechanism underlying the abnormal metabolism of tumor cells. We further found that the downregulated succinylation may result from decrease of succinyl-CoA level, which is the sole significantly downregulated product in TCA cycle (Fig. 2). As the donor of succinyl-CoA, α-ketoglutarate can be consumed for lipid synthesis under hypoxia (51). Additionally, hypoxia and HIF-1 activation promotes an alternative pathway of reductive carboxylation for citrate syntheses through a reverse flux of glutamine-derived α-ketoglutarate (52). In our study, we identified downregulation of AMPK and upregulation of ACC, which are suggested to contribute to a metabolic shift toward increased fatty acid synthesis in aggressive cancers (53). Together, α-ketoglutarate, a key regulator of metabolic shift in SHEEC, changes the direction of carbon flux to fatty acid synthesis, decreases the flux toward succinyl-CoA. Thus it is conceivable that abnormal metabolism under hypoxia decreases the level of succinyl-CoA, further leading to hyposuccinylation of proteins in SHEEC. On the other hand, our results also showed the effects of succinylation on the epigenetics in SHEEC. It has been reported the ratio of α-ketoglutarate/succinateis is able to control the activity of the demethylases (54), and hypersuccinylation can also regulate the histone methylation (40). In this work, large scale of histone PTMs profiling using quantitative mass spectrometry enables us to understand the relationship between succinylation and
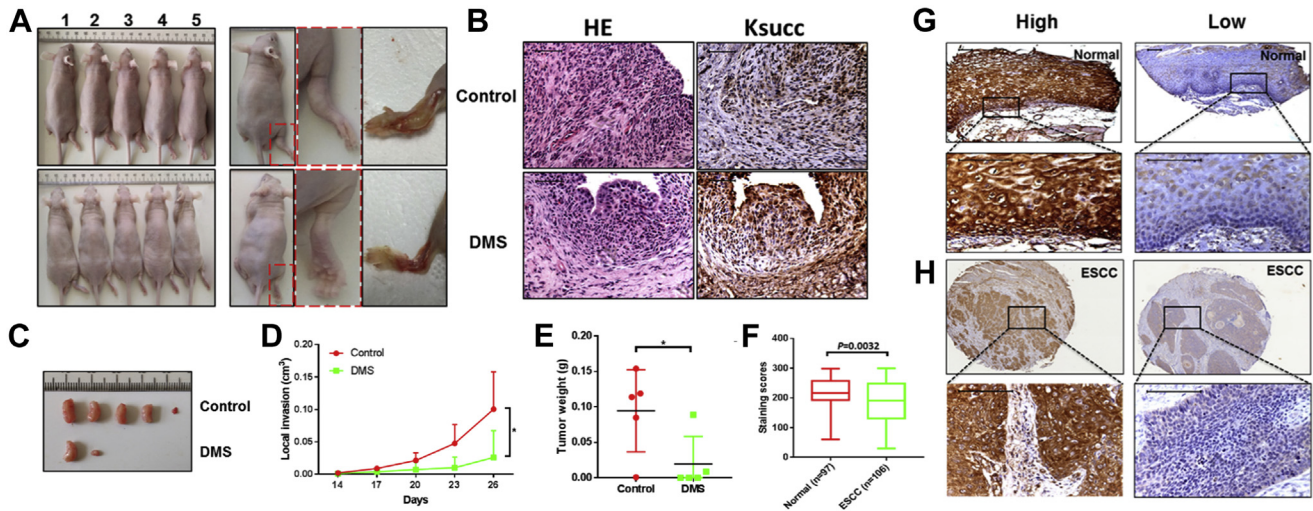
FIG. 6. **Hyposuccinylation enhanced migration and occurred in ESCC samples.** *A*, effect of DMS treatment on local tumor invasion *in vivo*. *Left*, photographs of tumorigenesis in SHEEC cells in xenograft mice; *right*, representative images of local invasion tumour volumes 30 days after footpad injection with the indicated cells. *B*, *Left*, hematoxylin and eosin-stained (HE) images of invaded tumors (scale bars = 50 μm); *right*, images of immunohistochemical of lysine succinylation in invaded tumors with or without injection. *C*, representative images of excised invasive tumor. *D*, invaded tumor size in each group over time following footpad injection with the indicated cells. *E*, tumor weight of invasive tumor. Data are shown as mean ± SD (n = 5), *$p < 0.05$. *F–H*, expression of lysine succinylation in ESCC and normal esophageal mucosa. Representative images of immunohistochemical staining for Ksucc in normal esophageal mucosa (*F*) and ESCC samples (*G*) Scale bars, 50 μm. *H*, box and whisker diagram showing the staining scores of Ksucc in normal esophageal mucosa and carcinoma samples. $p < 0.05$, independent-samples *t* test.

histone marks more comprehensively. Besides the positive regulation of succinylation in histone PTMs such as H3K4me1 and H4K20me1 reported previous, H3K9me2 was identified and verified to be negatively regulated by succinylation, as well as linked with the migration ability of esophageal cancer cell lines. Together, our work demonstrated that hyposuccinylation regulated SHEEC cell behavior on both metabolic and epigenetic levels.

To date, one of the bottlenecks in therapeutic development of ESCC has been the lack of viable therapeutic target (3). In this study, we identified hyposuccinylation in SHEEC and human primary ESCC specimens, and a significant correlation was observed between succinylation level and lymph node metastasis. Site-specific mutation of succinylation sites further confirmed that PTM can regulate the migration of ESCC cell lines. More importantly, restoration of lysine succinylation by addition of DMS inhibited the migration of ESCC both *in vitro* and *in vivo*. In addition, the abnormal succinylation was enriched in the metabolic enzymes, which themselves have been considered as potential targets for anticancer therapy (51). There results suggest the potential significance of the abnormal PTMs on the clinical management of ESCC.

CONCLUSIONS

In conclusion, our study provides a comprehensive resource of proteomics and PTMs for ESCC cells, identifies hyposuccinylation, and reveals abnormal metabolic processes

and epigenetic marks in ESCC. These changes lead to function alteration of substrates and finally regulate the migration of ESCC cell lines. This study also has the potential to enable new advances in succinylation associated diagnostics and therapeutics of ESCC.

ETHICS APPROVAL AND CONSENT TO PARTICIPATE

ESCC tissues used for immunohistochemical analysis were collected from Shantou Central Hospital with IRB approval (16-171/1250). Written informed consent was obtained from each patient included in this study.

DATA AVAILABILITY

The mass spectrometry proteomics data have been deposited to the ProteomeXchange Consortium (http://proteomecentral.proteomexchange.org) *via* the iProX partner repository with the data set identifier PXD021567 and PXD021700 (for histone PTM quantitation).

Supplemental data—This article contains supplemental data.

REFERENCES

1. Zhao, P., Dai, M., Chen, W. Q., and Li, N. (2010) Cancer trends in China. *Jpn. J. Clin. Oncol.* **40**, 281–285
2. Pennathur, A., Gibson, M. K., Jobe, B. A., and Luketich, J. D. (2013) Oesophageal carcinoma. *Lancet* **381**, 400–412
3. Song, Y. M., Li, L., Ou, Y. W., Gao, Z. B., Li, E. M., Li, X. C., Zhang, W. M., Wang, J. Q., Xu, L. Y., Zhou, Y., Ma, X. J., Liu, L. Y., Zhao, Z. T., Huang, X. L., Fan, J., *et al.* (2014) Identification of genomic alterations in oesophageal squamous cell cancer. *Nature* **509**, 91–95
4. Lin, D. C., Hao, J. J., Nagata, Y., Xu, L., Shang, L., Meng, X., Sato, Y., Okuno, Y., Varela, A. M., Ding, L. W., Garg, M., Liu, L. Z., Yang, H., Yin, D., Shi, Z. Z., *et al.* (2014) Genomic and molecular characterization of esophageal squamous cell carcinoma. *Nat. Genet.* **46**, 467–473
5. Lin, D. C., Wang, M. R., and Koeffler, H. P. (2018) Genomic and epigenomic aberrations in esophageal squamous cell carcinoma and implications for patients. *Gastroenterology* **154**, 374–389
6. Zhao, D., Zou, S. W., Liu, Y., Zhou, X., Mo, Y., Wang, P., Xu, Y. H., Dong, B., Xiong, Y., Lei, Q. Y., and Guan, K. L. (2013) Lysine-5 acetylation negatively regulates lactate dehydrogenase A and is decreased in pancreatic cancer. *Cancer Cell* **23**, 464–476
7. Sabari, B. R., Zhang, D., Allis, C. D., and Zhao, Y. (2017) Metabolic regulation of gene expression through histone acylations. *Nat. Rev. Mol. Cell Biol* **18**, 90–101
8. Portela, A., and Esteller, M. (2010) Epigenetic modifications and human disease. *Nat. Biotechnol.* **28**, 1057–1068
9. Zhang, K., Li, L. Y., Zhu, M. X., Wang, G. J., Xie, J. J., Zhao, Y. L., Fan, E. G., Xu, L. Y., and Li, E. M. (2015) Comparative analysis of histone H3 and H4 post-translational modifications of esophageal squamous cell carcinoma with different invasive capabilities. *J. Proteomics* **112**, 180–189
10. Aebersold, R., and Mann, M. (2016) Mass-spectrometric exploration of proteome structure and function. *Nature* **537**, 347–355
11. Choudhary, C., Kumar, C., Gnad, F., Nielsen, M. L., Rehman, M., Walther, T. C., Olsen, J. V., and Mann, M. (2009) Lysine acetylation targets protein complexes and co-regulates major cellular functions. *Science* **325**, 834–840
12. Mertins, P., Mani, D. R., Ruggles, K. V., Gillette, M. A., Clauser, K. R., Wang, P., Wang, X. L., Qiao, J. W., Cao, S., Petralia, F., Kawaler, E., Mundt, F., Krug, K., Tu, Z. D., Lei, J. T., *et al.* (2016) Proteogenomics connects somatic mutations to signalling in breast cancer. *Nature* **534**, 55–62
13. Sharma, K., D'Souza, R. C. J., Tyanova, S., Schaab, C., Wisniewski, J. R., Cox, J., and Mann, M. (2014) Ultradeep human phosphoproteome reveals a distinct regulatory nature of Tyr and Ser/Thr-based signaling. *Cell Rep.* **8**, 1583–1594
14. Noberini, R., Uggetti, A., Pruneri, G., Minucci, S., and Bonaldi, T. (2016) Pathology tissue-quantitative mass spectrometry analysis to profile histone post-translational modification patterns in patient samples. *Mol. Cell Proteomics* **15**, 866–877
15. Zhang, B., Kirov, S., and Snoddy, J. (2005) WebGestalt: An integrated system for exploring gene sets in various biological contexts. *Nucleic Acids Res.* **33**, W741–W748
16. Basu, S. S., and Blair, I. A. (2012) SILEC: A protocol for generating and using isotopically labeled coenzyme A mass spectrometry standards. *Nat. Protoc.* **7**, 1–11
17. Hu, H., Juvekar, A., Lyssiotis, C. A., Lien, E. C., Albeck, J. G., Oh, D., Varma, G., Hung, Y. P., Ullas, S., Lauring, J., Seth, P., Lundquist, M. R., Tolan, D. R., Grant, A. K., Needleman, D. J., *et al.* (2016) Phosphoinositide 3-kinase regulates glycolysis through mobilization of aldolase from the actin cytoskeleton. *Cell* **164**, 433–446
18. Xie, J. J. (2010) Involvement of CYR61 and CTGF in the Fascin-mediated proliferation and invasiveness of esophageal squamous cell carcinomas cells. *Am. J. Pathol.* **176**, 939–951
19. Li, C. Q., Huang, G. W., Wu, Z. Y., Xu, Y. J., Li, X. C., Xue, Y. J., Zhu, Y., Zhao, J. M., Li, M., Zhang, J., Wu, J. Y., Lei, F., Wang, Q. Y., Li, S., Zheng, C. P., *et al.* (2017) Integrative analyses of transcriptome sequencing identify novel functional lncRNAs in esophageal squamous cell carcinoma. *Oncogenesis* **6**, e297
20. Sidoli, S., Bhanu, N. V., Karch, K. R., Wang, X. S., and Garcia, B. A. (2016) Complete workflow for analysis of histone post-translational modifications using bottom-up mass spectrometry: From histone extraction to data analysis. *J. Vis. Exp.*, 54112
21. Yuan, Z.-F., Sidoli, S., Marchione, D. M., Simithy, J., Janssen, K. A., Szurgot, M. R., and Garcia, B. A. (2018) EpiProfile 2.0: A computational platform for processing epi-proteomics mass spectrometry data. *J. Proteome Res.* **17**, 2533–2541
22. Zhang, F. R., Tao, L. H., Shen, Z. Y., Lv, Z., Xu, L. Y., and Li, E. M. (2008) Fascin expression in human embryonic, fetal, and normal adult tissue. *J. Histochem. Cytochem.* **56**, 193–199
23. Xie, J. J., Xu, L. Y., Wu, Z. Y., Zhao, Q., Xu, X. E., Wu, J. Y., Huang, Q., and Li, E. M. (2011) Prognostic implication of Ezrin expression in esophageal squamous cell carcinoma. *J. Surg. Oncol.* **104**, 538–543
24. Levenson, R. M., Fornari, A., and Loda, M. (2008) Multispectral imaging and pathology: Seeing and doing more. *Expert Opin. Med. Diagn.* **2**, 1067–1081
25. Mansfield, J. R., Hoyt, C., and Levenson, R. M. (2008) Visualization of microscopy-based spectral imaging data from multi-label tissue sections. *Curr. Protoc. Mol. Biol.* Chapter 14:Unit 14.19
26. Zhang, X.-D., Huang, G.-W., Xie, Y.-H., He, J.-Z., Guo, J.-C., Xu, X.-E., Liao, L.-D., Xie, Y.-M., Song, Y.-M., and Li, E.-M. (2017) The interaction of lncRNA EZR-AS1 with SMYD3 maintains overexpression of EZR in ESCC cells. *Nucleic Acids Res.* **46**, 1793–1809
27. Sun, J. C., Yan, J. Q., Yuan, X. Z., Yang, R. N., Dan, T. Y., Wang, X. S., Kong, G. Q., and Gao, S. G. (2016) A computationally constructed ceRNA interaction network based on a comparison of the SHEE and SHEEC cell lines. *Cell Mol. Biol. Lett.* **21**, 21

28. Shgn, Z., Cen, S., and Zeng, Y. (1999). Immortalization of human fetal esophageal epithelial cells induced by E6 and E7 genes of human papilloma virus 18 *Zhonghua Shi Yan He Lin Chuang Bing Du Xue Za Zhi* **13**, 121–123

29. Abreu, R. D., Penalva, L. O., Marcotte, E. M., and Vogel, C. (2009) Global signatures of protein and mRNA expression levels. *Mol. Biosyst.* **5**, 1512–1526

30. Li, L. Y., Zhang, K., Jiang, H., Xie, Y. M., Liao, L. D., Chen, B., Du, Z. P., Zhang, P. X., Chen, H., Huang, W., Jia, W., Cao, H. H., Zheng, W., Li, E. M., and Xu, L. Y. (2015) Quantitative proteomics reveals the down-regulation of GRB2 as a prominent node of F806-targeted cell proliferation network. *J. Proteomics* **117**, 145–155

31. Papandreou, I., Cairns, R. A., Fontana, L., Lim, A. L., and Denko, N. C. (2006) HIF-1 mediates adaptation to hypoxia by actively downregulating mitochondrial oxygen consumption. *Cell Metab.* **3**, 187–197

32. Tannahill, G. M., Curtis, A. M., Adamik, J., Palsson-McDermott, E. M., McGettrick, A. F., Goel, G., Frezza, C., Bernard, N. J., Kelly, B., Foley, N. H., Zheng, L., Gardet, A., Tong, Z., Jany, S. S., Corr, S. C., *et al.* (2013) Succinate is an inflammatory signal that induces IL-1beta through HIF-1alpha. *Nature* **496**, 238–242

33. Zhao, E. D., Maj, T., Kryczek, I., Li, W., Wu, K., Zhao, L. L., Wei, S., Crespo, J., Wan, S. S., Vatan, L., Szeliga, W., Shao, I., Wang, Y., Liu, Y., Varambally, S., *et al.* (2016) Cancer mediates effector T cell dysfunction by targeting microRNAs and EZH2 via glycolysis restriction. *Nat. Immunol.* **17**, 95–103

34. Semenza, G. L. (2013) HIF-1 mediates metabolic responses to intratumoral hypoxia and oncogenic mutations. *J. Clin. Invest.* **123**, 3664–3671

35. Koppenol, W. H., Bounds, P. L., and Dang, C. V. (2011) Otto Warburg's contributions to current concepts of cancer metabolism. *Nat. Rev. Cancer* **11**, 325–337

36. Du, J. T., Zhou, Y. Y., Su, X. Y., Yu, J. J., Khan, S., Jiang, H., Kim, J., Woo, J., Kim, J. H., Choi, B. H., He, B., Chen, W., Zhang, S., Cerione, R. A., Auwerx, J., *et al.* (2011) Sirt5 is a NAD-dependent protein lysine demalonylase and desuccinylase. *Science* **334**, 806–809

37. Park, J., Chen, Y., Tishkoff, D. X., Peng, C., Tan, M. J., Dai, L. Z., Xie, Z. Y., Zhang, Y., Zwaans, B. M. M., Skinner, M. E., Lombard, D. B., and Zhao, Y. M. (2013) SIRT5-Mediated lysine desuccinylation impacts diverse metabolic pathways. *Mol. Cell* **50**, 919–930

38. Weinert, B. T., Scholz, C., Wagner, S. A., Iesmantavicius, V., Su, D., Daniel, J. A., and Choudhary, C. (2013) Lysine succinylation is a frequently occurring modification in prokaryotes and eukaryotes and extensively overlaps with acetylation. *Cell Rep.* **4**, 842–851

39. Han, T. Y., Kang, D., Ji, D. K., Wang, X. Y., Zhan, W. H., Fu, M. G., Xin, H. B., and Wang, J. B. (2013) How does cancer cell metabolism affect tumor migration and invasion? *Cell Adhes. Migr.* **7**, 395–403

40. Li, F., He, X., Ye, D., Lin, Y., Yu, H., Yao, C., Huang, L., Zhang, J., Wang, F., Xu, S., Wu, X., Liu, L., Yang, C., Shi, J., He, X., *et al.* (2015) NADP(+)-IDH mutations promote hypersuccinylation that impairs mitochondria respiration and induces apoptosis resistance. *Mol. Cell* **60**, 661–675

41. Leithner, K., Hrzenjak, A., Trotzmuller, M., Moustafa, T., Kofeler, H. C., Wohlkoenig, C., Stacher, E., Lindenmann, J., Harris, A. L., Olschewski, A., and Olschewski, H. (2015) PCK2 activation mediates an adaptive response to glucose depletion in lung cancer. *Oncogene* **34**, 1044–1050

42. Kaelin, W. G. (2014) DisABLing kidney cancers caused by fumarate hydratase mutations. *Cancer Cell* **26**, 779–780

43. Spiegel, K., Pines, O., Ta-Shma, A., Burak, E., Shaag, A., Halvardson, J., Edvardson, S., Mahajna, M., Zenvirt, S., Saada, A., Shalev, S., Feuk, L., and Elpeleg, O. (2012) Infantile cerebellar-retinal degeneration associated with a mutation in mitochondrial aconitase, ACO2. *Am. J. Hum. Genet.* **90**, 518–523

44. Yuan, Z. F., Lin, S., Molden, R. C., Cao, X. J., Bhanu, N. V., Wang, X. S., Sidoli, S., Liu, S. C., and Garcia, B. A. (2015) EpiProfile quantifies histone peptides with modifications by extracting retention time and intensity in high-resolution mass spectra. *Mol. Cell Proteomics* **14**, 1696–1707

45. Sullivan, L. B., Gui, D. Y., and Heiden, M. G. (2016) Altered metabolite levels in cancer: Implications for tumour biology and cancer therapy. *Nat. Rev. Cancer* **16**, 680–693

46. Gottlieb, E., and Tomlinson, I. P. M. (2005) Mitochondrial tumour suppressors: A genetic and biochemical update. *Nat. Rev. Cancer* **5**, 857–866

47. Dang, L., White, D. W., Gross, S., Bennett, B. D., Bittinger, M. A., Driggers, E. M., Fantin, V. R., Jang, H. G., Jin, S., Keenan, M. C., Marks, K. M., Prins, R. M., Ward, P. S., Yen, K. E., Liau, L. M., *et al.* (2009) Cancer-associated IDH1 mutations produce 2-hydroxyglutarate. *Nature* **462**, 739–U752

48. Zhou, L., Wang, F., Sun, R., Chen, X., Zhang, M., Xu, Q., Wang, Y., Wang, S., Xiong, Y., Guan, K. L., Yang, P., Yu, H., and Ye, D. (2016) SIRT5 promotes IDH2 desuccinylation and G6PD deglutarylation to enhance cellular antioxidant defense. *EMBO Rep.* **17**, 811–822

49. Thompson, C. B. (2009) Metabolic enzymes as oncogenes or tumor suppressors. *N. Engl. J. Med.* **360**, 813–815

50. Hu, J., Locasale, J. W., Bielas, J. H., O'Sullivan, J., Sheahan, K., Cantley, L. C., Vander Heiden, M. G., and Vitkup, D. (2013) Heterogeneity of tumor-induced gene expression changes in the human metabolic network. *Nat. Biotechnol.* **31**, 522–529

51. Metallo, C. M., Gameiro, P. A., Bell, E. L., Mattaini, K. R., Yang, J., Hiller, K., Jewell, C. M., Johnson, Z. R., Irvine, D. J., Guarente, L., Kelleher, J. K., Vander Heiden, M. G., Iliopoulos, O., and Stephanopoulos, G. (2012) Reductive glutamine metabolism by IDH1 mediates lipogenesis under hypoxia. *Nature* **481**, 380–384

52. The Cancer Genome Atlas Research Network. (2013) Comprehensive molecular characterization of clear cell renal cell carcinoma. *Nature* **499**, 43–49

53. Ward, P. S., and Thompson, C. B. (2012) Metabolic reprogramming: A cancer hallmark even warburg did not anticipate. *Cancer Cell* **21**, 297–308

54. Michealraj, K. A., Kumar, S. A., Kim, L. J. Y., Cavalli, F. M. G., Przelicki, D., Wojcik, J. B., Delaidelli, A., Bajic, A., Saulnier, O., MacLeod, G., Vellanki, R. N., Vladoiu, M. C., Guilhamon, P., Ong, W. N., Lee, J. J. Y., *et al.* (2020) Metabolic regulation of the epigenome drives lethal infantile ependymoma. *Cell* **181**, 1329–1345.e24